ADVANCED FUNCTIONAL MATERIALS
www.afm-journal.de

Electronic Structure and Geminate Pair Energetics at Organic–Organic Interfaces: The Case of Pentacene/ C_{60} Heterojunctions

By *Stijn Verlaak, David Beljonne, David Cheyns, Cedric Rolin, Mathieu Linares, Frédéric Castet, Jérôme Cornil,* and *Paul Heremans**

Organic semiconductors are characterized by localized states whose energies are predominantly determined by electrostatic interactions with their immediate molecular environment. As a result, the details of the energy landscape at heterojunctions between different organic semiconductors cannot simply be deduced from those of the individual semiconductors, and they have so far remained largely unexplored. Here, microelectrostatic computations are performed to clarify the nature of the electronic structure and geminate pair energetics at the pentacene/C_{60} interface, as archetype for an interface between a donor molecule and a fullerene electron acceptor. The size and orientation of the molecular quadrupole moments, determined by material choice, crystal orientation, and thermodynamic growth parameters of the semiconductors, dominate the interface energetics. Not only do quadrupoles produce direct electrostatic interactions with charge carriers, but, in addition, the discontinuity of the quadrupole field at the interface induces permanent interface dipoles. That discontinuity is particularly striking for an interface with C_{60} molecules, which by virtue of their symmetry possess no quadrupole. Consequently, at a pentacene/C_{60} interface, both the vacuum-level shift and geminate pair dissociation critically depend on the orientation of the pentacene π-system relative to the adjacent C_{60}.

1. Introduction

One of the features differentiating organic semiconductors from their inorganic counterparts is the localized nature of excess charge carriers and excited states. Excess charges and excited states at room temperature can be thought of being localized on an individual small-molecule or polymer site, rather than being delocalized as they are in crystalline silicon.[1] The probability for an excess charge sitting on one molecule to jump to a neighboring molecule is low in organic materials, such that those charges will (mainly electronically) polarize their environment before having made the jump, resulting in a polaron state. This polaron is even more unlikely to jump to a neighboring site since the charge is now dressed by its polarized environment. The polaron is therefore the relevant charge transport species which determines the energy level for transport of excess charges.[2] Similarly, absorption of light in organic semiconductors results in the generation of localized electronic excitations—referred to as polaron-excitons—rather than free electron–hole pairs as produced in many inorganic semiconductors. Organic optoelectronic devices such as solar cells take great benefit of interfaces between different organic semiconductors in order to manipulate excitons and polarons, amongst others to split the neutral excitons into free charge carriers. Unfortunately, the exact details of the energetic landscape near an organic semiconductor hetero-interface, and its implications for the dynamics of charge dissociation and recombination, remain largely unexplored.

In pristine organic semiconductors—being small-molecule materials or polymers—an exciton has a chance to dissociate into free polarons only when it is "hot".[2,3] Excess energy of the exciting photon can be used to propel the excited electron and hole away from each other. The unthermalized electron and hole are initially too fast to polarize their environment and move with high mobility, but are slowed down by scattering with the matrix until they settle as polarons. If those polarons have thermalized sufficiently far from each other to escape their mutual Coulombic attraction, they are free to travel independently from each other. Many polarons

[*] Prof. P. Heremans, Dr. S. Verlaak, Dr. D. Cheyns, C. Rolin
IMEC vzw
Kapeldreef 75, 3001 Leuven (Belgium)
E-mail: paul.heremans@imec.be
Prof. P. Heremans
ESAT, Katholieke Universiteit Leuven
Kasteelpark Arenberg 10
B-3001 Leuven (Belgium)
Dr. D. Beljonne, Dr. J. Cornil
Chemistry of Novel Materials
University of Mons Hainaut
20, Place du Parc, 7000 Mons (Belgium)
Dr. M. Linares
Department of Physics, Chemistry and Biology, IFM
Linköping University
581 83 Linköping (Sweden)
Dr. F. Castet
Institut des Sciences Moleculaires
Université Bordeaux I
351 cours de la Liberation, 33405 Talence (France)

DOI: 10.1002/adfm.200901233

will not succeed in doing so, however, and will form a Coulombically bound geminate pair. Such a "cold" geminate pair has a much lower probability for dissociation into free polarons, and may eventually recombine.

Those concepts have been adopted to describe photogeneration in organic solar cells.[4,5] There, an interface between an electron-donor and an electron-acceptor material is used to greatly enhance dissociation of excitons (which in general were generated in the bulk and diffused towards the interface, so that those excitons are thermalized). An excited electron in the donor can "tumble" down into the lower-lying electron-transport level of the acceptor (or an excited hole in the acceptor can fall into a lower-lying hole-transport level of the donor). The excess energy that needs to be spilled before the electron (hole) has thermalized into a polaron with the energy of the electron- (hole-) transport level of the acceptor (donor) can again be used to separate both polarons. This process is increasingly efficient when assisted by an electric field,[2,6] and is a plausible mechanism to explain the increased photogeneration efficiency in reverse-biased organic solar cells.[4,7] If the electron in the acceptor thermalizes within the attraction well of the hole in the donor material, however, both charge carriers will Coulombically bind as a geminate pair, localized at the interface. This thermalized pair is difficult to break.[8] In practice, geminate pair dynamics (dissociation and recombination) and energetics dominate open-circuit conditions in organic solar cells.[9–11] Note that for polymer-based solar cells, reverse-bias conditions are sometimes interpreted in terms of geminate-pair dissociation instead of hot exciton dissociation mechanisms.[7] In any case, it is clear that a more profound understanding of geminate-pair properties will contribute to better insight into the function, design, and optimization of organic solar cells.

Similarly to polarons, the energetics and dynamics of geminate pairs are largely dominated by the electrostatic interactions of the charges with their surrounding environment. These can be calculated accurately using micro-electrostatic methods.[2,12–15] In the present work, we will use micro-electrostatics to give a detailed energetic description of the pentacene/C_{60} interface. Pentacene and C_{60} are archetypical materials, whose heterojunction forms a reasonably well-characterized donor–acceptor pair used in devices.[16–18] Our results provide new insights into the physics of such organic donor–acceptor interfaces, and most importantly on geminate pair dissociation at such interfaces.

2. Results and Discussion

2.1. The Pentacene–C_{60} Heterojunction

In bulk organic crystals, the transport levels of positive and negative polarons differ from the highest occupied molecular orbital (HOMO) and lowest unoccupied molecular orbital (LUMO) energy of the molecule in the gas phase, respectively. The main contribution to this difference comes from electrostatic interactions between the excess charge in the solid phase and the π-electrons of its surrounding molecules. First of all, dipoles are induced by the polarization of those neighboring π-orbitals and stabilize the charge irrespective of its sign. Second, conjugated molecules such as pentacene feature a quadrupolar charge distribution with partial positive charges in the plane and negative π-electronic charges above and below the plane. Those quadrupoles are present permanently, and the corresponding electrostatics will either stabilize or destabilize a nearby charge, depending on its sign and relative position. A last but small contribution to the difference between gas phase HOMO/LUMO and the solid phase transport levels stems from the nuclear relaxation of the charged molecule and its matrix.[2,12] For pentacene, as well as for several other organic crystals, this mainly electrostatic model provides a very satisfactory explanation for the experimentally observed differences between gas phase HOMO (LUMO) and solid phase hole (electron) transport level energies.[2,13] Reference [13] compares the electrostatic model used here with more recent models. Figure 1 sketches relevant interaction energies. For C_{60}, this electrostatic description has not been validated yet. Because of its symmetry and closed-shell electronic structure, the molecular quadrupole moment of C_{60} is zero, and the intramolecular nuclear relaxation energy is very small (around 0.024 eV).[19] What is left is the charge-induced dipole (or polarization) energy to bridge the gap between the gas phase LUMO and the electron transport level energy. Experimentally, this gap amounts to 0.95 eV.[20] The present microelectrostatic calculation yields a value of 0.92 eV for the polarization energy. After addition of the nuclear relaxation energy (0.024 eV), the calculated value of 0.944 eV compares well to the experimental value of 0.95 eV.

At interfaces between two organic semiconductors, the microelectrostatic environment is different from that in the bulk of any of the two organic semiconductors. Both molecular polarizability and molecular quadrupole moment will vary abruptly across the interface. Consequently, both charge-induced dipole and charge-quadrupole interaction energies are expected to vary near the interface. Discontinuities in charge-induced dipole interaction energies are fairly restricted, considering the limited differences in dielectric constants and hence polarizability in organic materials ($\varepsilon_{\text{pentacene}} = 3$ and $\varepsilon_{C60} = 4$) as well as the fact that all induced

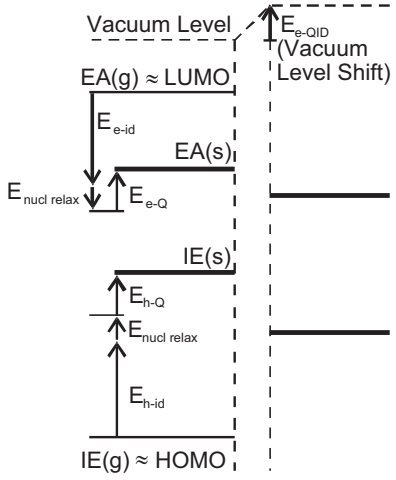

Figure 1. Sketch of relevant interaction energies E between holes (h) or electrons (e) and quadrupoles (Q), induced dipoles (id), and quadrupole-induced interface dipoles (QIDs).Those energies determine the difference between the gas (g) and solid phase (s) electron affinities (EA) and between the gas and solid phase ionization energies (IE).

dipoles will always stabilize their inducing charge irrespective of which side of the interface they are induced. On the other hand, variations in charge–quadrupole interaction energies can be more substantial: molecular quadrupole moments are clearly present in most planar aromatic molecules such as pentacene, yet are zero for spherical symmetric molecules such as C_{60}. Equally important is the fact that quadrupoles can not only stabilize but also destabilize a charge, depending on the orientation of the quadrupole relative to the charge. Abrupt changes in molecular quadrupole moment and its orientation across an interface can therefore significantly impact its interaction with a charge in the vicinity of the interface. The impact of the interface on charge-induced dipole and charge–quadrupole interaction energies will fade out with increasing distance to the interface, however, until polarons reach their bulk energies.

2.2. Structure and Calculations

We calculated the charge-induced dipole interaction energy (i.e., the polarization energy) as well as the charge–quadrupole interaction energy for the pentacene/C_{60} interface. To assess the impact of molecular orientation near the interface, two different pentacene surfaces were considered to interface with a C_{60} (001) surface: the pentacene (01–1) surface, which is characterized by a high density of π-orbitals exposed to the surface, and the pentacene (001) surface, which exposes its C−H bonds to the surface. While the latter corresponds to the lowest energy surface of the pentacene equilibrium crystal and is therefore abundantly present in pentacene crystals and grains,[21] the former surface was chosen to highlight the impact of π-orbitals on interfacial processes. The interfaces were assembled by optimizing the interfacial energy of two approaching rigid crystal surfaces using the molecular mechanics MM3 force field. The assemblies are shown in Figure 2. The polarization and charge–quadrupole interaction energies are plotted in Figure 3. Figure 3 clearly shows that the interaction energies respond more vigorously to the (01–1) interface than to the (001) interface. Intuitively, this is because the (01–1) exposes its electrostatically 'reactive' π-orbitals to the interface (i.e., its polarizability and quadrupole moment), while the (001) shields its π-orbitals from the interface. Most importantly, it is seen from Figure 3 that owing to the uncompensated quadrupoles at the interface, the positive and negative charges experience an electrostatic potential that is repulsive in the (01–1) case and attractive in the (001) case. In other words, the interfacial quadrupolar field is expected to assist charge separation at the interface with the (01–1) pentacene crystal surface while it is favorable to charge recombination at the interface with the (001) plane.

In contrast to the early view that the electronic structures of thin film layers would simply line up, ultraviolet photoelectron spectroscopy (UPS) measurements show that the energy level alignment of organic/organic interfaces is often controlled by the formation of an interfacial dipole (as found for metal–organic layers), resulting in a vacuum-level shift.[22,23] Interfacial dipoles originate from partial or integer charge transfer from the donor to the acceptor, or from polarization effects induced by an asymmetric electronic density distribution over the donor and the acceptor.[24] In some organic–organic interface systems, ground state charge transfer was found to be an important factor, for example in references [13,25,26]. For the present case, however, quantum-chemical calculations using density functional theory at the B3LYP/6-31G(d) level rule out any significant ground-state charge-transfer at the pentacene/C_{60} model interfaces. Interface dipoles can be expected as a consequence of the presence of molecular quadrupoles in pentacene molecules and their absence in C_{60} molecules. The abrupt imbalance in molecular quadrupoles generates an electric field across the interface. This field in turn polarizes the pentacene and C_{60} molecules near the interface, that is, dipoles are induced on those molecules. Since the quadrupoles are permanent in nature, those quadrupole-induced interface dipoles (QIDs) are permanent as well. Notice that such quadrupole-induced dipoles do also form near surfaces (interfaces between organic semiconductors and vacuum), leading to a change in the ionization potential as a function of molecular packing.[27] The results of micro-electrostatic calculations are reported in Figure 4, namely the hole–QID interaction energy. Note that the electron–QID interaction energy (i.e., the vacuum level shift) is equal in magnitude but opposite in sign to the hole–QID interaction (a permanent dipole that stabilizes a hole will destabilize an electron).

A remarkable difference is noticeable when comparing the vacuum level shifts of the two interfaces studied. As a result of the different orientation of the pentacene molecules relative to the interface, the sign of the vacuum level shift reverses when going from the pentacene(001)/C_{60} to the pentacene (01–1)/C_{60} interfaces. The reversal of the polarity of the vacuum level shift has been experimentally observed for the phthalocyanine/C_{60} interface as compared to the C_{60}/phthalocyanine interface, that is, upon swapping the deposition sequence, but has remained unexplained so far.[28] The present results suggest that for different deposition sequences, different crystal orientations of the phthalocyanine layer are obtained with respect to the C_{60} layer, thus

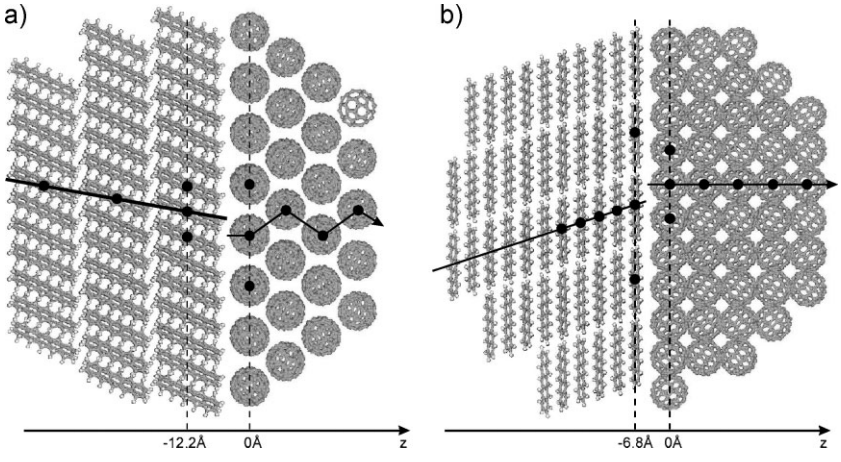

Figure 2. a) the pentacene(001)/C60(001) interface; b) the pentacene(01–1)/C60(001) interface. The dots denote the molecules for which simulation results are shown.

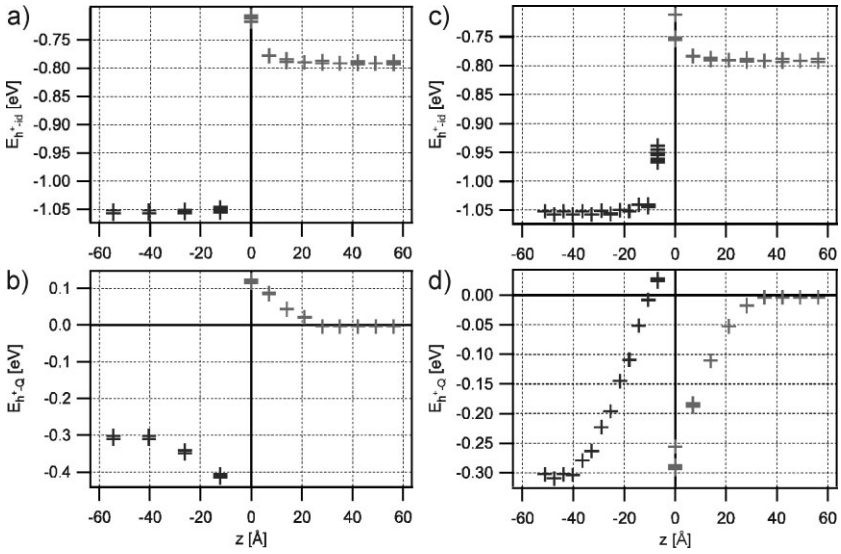

Figure 3. a) hole-induced dipole interaction (polarization) energy $E_{h\text{-id}}$ for the pentacene(001)/C_{60}(001) interface versus distance to the interface; b) hole–quadrupole interaction energy $E_{h\text{-Q}}$ for the pentacene(001)/C_{60}(001) interface versus distance to the interface; c) hole-induced dipole interaction energy for the pentacene(01–1)/C_{60}(001) interface; d) hole-quadrupole interaction energy for the pentacene(01–1)/C_{60}(001) interface. Z-axis as indicated in Figure 2. Negative energies stabilize the charge; positive energies destabilize the charge. Electron-induced dipole interaction energies are identical (dipoles induced by a hole will stabilize the hole; dipoles induced by an electron will have the same magnitude but opposite direction, to stabilize the electron). Electron–quadrupole interaction energies are the reverse of the hole–quadrupole interaction energies (permanent quadrupoles that stabilize a hole will destabilize an electron).

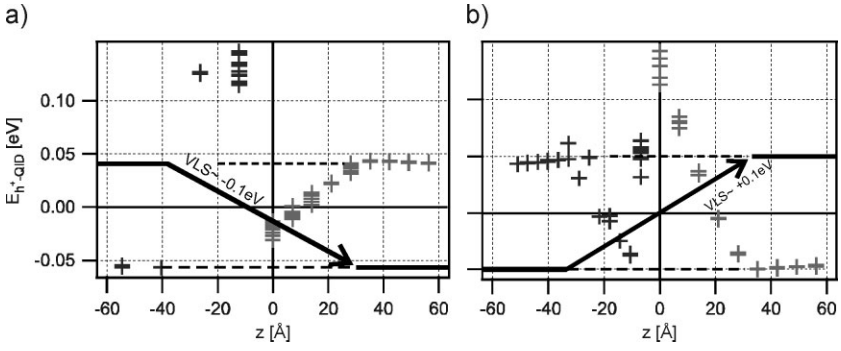

Figure 4. Hole–quadrupole-induced interface dipole interaction energy $E_{h\text{-QID}}$ near a) the pentacene(001)/C_{60} interface and b) the pentacene(01–1)/C_{60} interface. Each '+' represents the hole–QID interaction energy for the hole on a molecule with the corresponding z-value (see Figure 2). The vacuum-level shift (VLS) is related to $E_{h\text{-QID}}$. While the charge–QID interaction energy varies wildly near the interface, its value stabilizes away from the interface. The vacuum level shift is the difference between the stabilized values.

leading to differently oriented quadrupole-induced interface dipoles and a reversed polarity of the vacuum-level shift. A similar reversal of polarity of the vacuum-level shift upon inverting the deposition sequence was experimentally observed for the pentacene/C_{60} interface.[29] Moreover, the magnitudes of the observed vacuum-level shifts for interfaces between pentacene and C_{60} (0.11 eV and 0.07 eV depending on deposition sequence) correspond well to those calculated here.

When collecting all bulk and interfacial contributions to the energetics of charges in pentacene/C_{60}, the transport energies for positive and negative polarons approximately equal the solid phase ionization energy (IE(s)) and electron affinity (EA(s)) respectively, which can be written:

$$\mathrm{IE(s)} = \mathrm{IE(g)} + \mathrm{E_{h-id}} + \mathrm{E_{h-Q}} + \mathrm{E_{h-QID}} \qquad (1)$$

$$-\mathrm{EA(s)} = -\mathrm{EA(g)} + \mathrm{E_{e-id}} + \mathrm{E_{e-Q}} + \mathrm{E_{e-QID}}$$

with $E_{h\text{-id}}$ the hole-induced dipole interaction energy, $E_{h\text{-Q}}$ the hole–quadrupole interaction energy, and $E_{h\text{-QID}}$ the hole–quadrupole-induced interface dipole interaction energy. IE(g) and EA(g) are the gas-phase ionization energy and electron affinity respectively. The electron interaction energies are given by $E_{e\text{-id}} = +E_{h\text{-id}}$, $E_{e\text{-Q}} = -E_{h\text{-Q}}$, $E_{e\text{-QID}} = -E_{h\text{-QID}}$. The ionization energies and electron affinities are positive quantities by definition, and interaction energies are defined to have a negative sign when they stabilize the charge. This results in the energy diagrams for "free" excess charges as a function of the distance to the interface, shown in Figure 5. As expected, the more (electrostatically) "reactive" pentacene(01–1)/C_{60} interface displays more drastic deviations from the simple level alignment picture than the "inert" pentacene(001)/C_{60} interface. In particular, the electrostatic interactions between the positive charge on pentacene (negative charge on C_{60}) and the quadrupolar field at the interface drive the charges away from the pentacene(01–1)/C_{60} interface.

2.3. Discussion

A geminate pair can be viewed as a pair of an excess electron on C_{60} bound to an excess hole on pentacene. Since hole and electron polarize their environment together, they are more than just the sum of two polarons: the geminate pair should be viewed as a separate entity. The interaction energy between a geminate pair and permanent quadrupoles can therefore simply be calculated as $E_{gp\text{-Q}} = E_{h\text{-Q}} + E_{e\text{-Q}}$, while the interaction energy between a geminate pair and permanent interface dipoles is given by $E_{gp\text{-QID}} = E_{h\text{-QID}} + E_{e\text{-QID}}$. Note however that the hole and the electron are located at different molecules, so their interaction energies do not cancel out. The interaction energy between a geminate pair and the dipoles induced by this pair, $E_{gp\text{-id}}$, cannot be viewed as a sum of $E_{h\text{-id}}$ and $E_{e\text{-id}}$ because the dipoles induced by the "hole part" of the geminate pair are not independent from the dipoles induced by the "electron part" of the geminate pair. Therefore, $E_{gp\text{-id}}$ needs to be calculated separately using the same

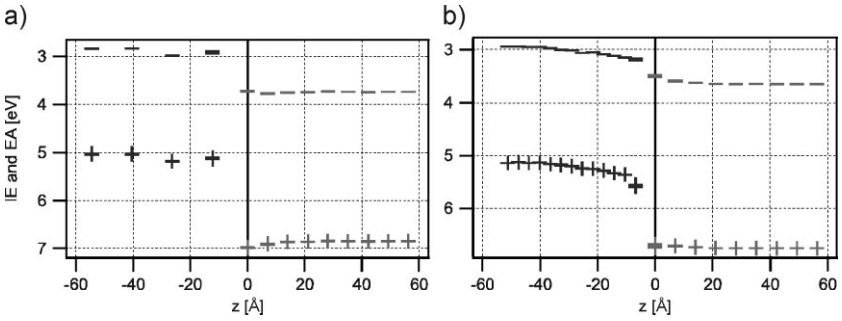

Figure 5. Computed energy diagrams of a) the pentacene(001)/C60 interface and b) the pentacene(01–1)/C60 interface.

microelectrostatic model. In addition to those interaction energies, the hole and electron in a geminate pair are attracted to each other by the Coulomb interaction energy $E_{e\text{-}h}$ (note that the Coulomb law is applied without dielectric screening, since this latter effect is already accounted for by the polarization energy). The geminate pair energies are tabulated in Table 1 for both interfaces studied. For comparison, the energies are shown for a hole (electron) located at a pentacene (C_{60}) molecule far away from the interface. For the pentacene(001)/C_{60} interface, a comparison of the total electrostatic interaction energy between the geminate pair and its environment (−2.685 eV) with the total electrostatic interaction energy of the separated electron–hole pair (−2.247 eV) shows that the geminate pair is more stable. A barrier of 0.438 eV needs to be overcome before the geminate pair can split into separate charges. In other words, recombination of a free electron and a free hole into a geminate pair is energetically favored in this case. In contrast, at the pentacene(01–1)/C_{60} interface, the geminate pair is equally stable as the separated charges and geminate pair splitting can easily occur. In the latter case, the bound electron and hole can approach closer together since the center of the pentacene molecule is much closer to the C_{60} molecule. This leads to a larger Coulombic attraction, yet a smaller interaction with induced dipoles: the closer the bound electron and hole, the more they appear as a neutral entity, which translates into smaller induced dipoles in the environment and subsequently lower polarization energy. Most strikingly, differences in quadrupole interactions significantly influence the stability of charges near the interface and in the bulk. We found that the asymmetry in electron density between pentacene and C_{60} induces an unexpected driving force for polaron pair dissociation at the reactive pentacene(01–1) surface. That finding is key to explaining why exciton dissociation can be so efficient at the interface between many donor molecules, featuring strong quadrupole moments, and fullerenes.

3. Conclusions

In conclusion, we have demonstrated the impact of material choice and crystal orientation on the electronic properties of organic–organic interfaces. Both size and orientation of the molecular quadrupoles of the interfacing materials play an important role in electrostatically influencing interface dipoles and vacuum level shift, and excess charge and geminate pair energetics. The size of the molecular quadrupole moment can be engineered by material choice: while most planar aromatic hydrocarbons have a net molecular quadrupole moment, symmetric spherical molecules such as C_{60} show only higher multipoles. The orientation of the molecular quadrupoles near the interface can in principle be engineered by influencing growth thermodynamics, either through growth parameters and/or by material (crystal) selection. As a rule of thumb, exposing electrostatically active π-orbitals towards the interface leads to a more profound impact on the electronic structure, the many details of which, however, need to be calculated microelectrostatically.

4. Experimental

All calculations were performed using a home-written Matlab toolbox described previously [13,30].

Heterojunction aggregates were constructed by gluing two rigid crystalline aggregates together along the appropriate crystal planes. The distance between the first pentacene monolayer and the first C_{60} monolayer nearest to the interface was optimized using the MM3 molecular mechanics force field. Translation and rotation of the C_{60} aggregate relative to the interface was optimized very crudely. The result of this procedure is a pentacene/C_{60} aggregate with a sharp interface along the desired crystal surfaces and with relevant intermolecular distances, yet without quasi-epitaxial alignment or interfacial relaxation.

Table 1. Interaction energies for a geminate pair near the interface, and a distant pair separated by the interface, for both the pentacene(001)/C_{60} interface and the pentacene(01–1)/C_{60} interface. Whenever possible, the contributions from the hole and the electron are mentioned separately.

		Geminate pair (hole on interfacial pentacene, electron on nearest C_{60})	Hole on pentacene away from interface, electron on C_{60} away from interface
Pentacene(001)/C_{60}	Coulomb energy	−1.114 eV	0 eV
	Induced dipole interaction	−1.188 eV	−1.058(h) −0.791(e) eV
	Quadrupole interaction	−0.415(h) −0.119(e) eV	−0.310(h) +0.004(e) eV
	QID interaction	+0.132(h) +0.019(e) eV	−0.053(h) −0.039(e) eV
	Total	−2.685 eV	−2.247 eV
Pentacene(01–1)/C_{60}	Coulomb energy	−1.732 eV	0 eV
	Induced dipole interaction	−0.593 eV	−1.052(h) −0.792(e) eV
	Quadrupole interaction	+0.025(h) +0.284(e) eV	−0.302(h) +0.004(e) eV
	QID interaction	+0.053(h) −0.128(e) eV	+0.043(h) +0.044(e) eV
	Total	−2.091 eV	−2.055 eV

Microelectrostatic calculations were performed as described previously [13]. Molecular quadrupole moments and excess charges were distributed equally over all π-carbon atoms in every molecule. It was verified that charge–quadrupole interactions were indeed negligible in C_{60}, by assigning radially oriented atomic quadrupole moments (equal in magnitude to typical oligoacene ''atomic'' quadrupole moments) to each of the carbon atoms in C_{60}. Therefore, the molecular quadrupole moment of C_{60} was set to zero. The molecular polarizability tensor of every pentacene molecule was distributed equally over the centers of the five aromatic rings. It has been previously shown that this is sufficiently accurate [13]. The molecular polarizability tensor of every C_{60} molecule was distributed over the centers of the 12 five-carbon rings in C_{60}, such that the radial and tangent contributions remained constant and that the sum of the 12 ''sub-molecular'' polarizability tensors gave the known C_{60} molecular polarizability tensor, i.e., an isotropic polarizability volume of 80 $Å^3$. This value of the polarizability volume is the result of an excellent agreement between ab initio calculations at the B3LYP level using a standard basis set (6-311 + G(d,p) (5D, 7F)), an estimate based on the macroscopic dielectric constant of 4 using the Claussius-Mosotti relation [19], and other estimates in literature [31].

To check the validity of the present microelectrostatic method for bulk C_{60}, values for the charge-induced dipole and the charge–quadrupole interaction energy were obtained for infinitely large C_{60} aggregates by proper extrapolation of the results for finite-sized aggregates, as described previously [13]. All other (interfacial) values were based on calculations using spherical aggregates that count typically ~500 molecules for self-consistent calculations (those involving induced dipoles) and that count up ~10 000 molecules for calculations that do not need to be performed self-consistently (those involving only permanent quadrupoles or permanent dipoles). As a result of the use of finite-size aggregates for the computations, there is a truncation error in all reported values. Given various scaling relations, this error is expected to be around 10% for charge-induced dipole interaction energies, and significantly smaller for charge–quadrupole interaction energies [13].

QIDs were calculated self-consistently within a spherical aggregate 6 nm in diameter, centered at the interface, using the fields coming from quadrupoles within a co-centric spherical aggregate 10 nm in diameter. Multiple such calculations were used to compute all quadrupole-induced interface dipoles within a cylinder with diameter 20 nm centered at the interface and protruding 3 nm at both sides of the interface. For each monolayer in this 6-nm-high and 20-nm-diameter cylinder, the quadrupole-induced interface dipoles were averaged. Per monolayer, the averaged dipole was imposed outside this 20-nm cylinder for radii smaller than 40 nm. Overall, a representative sheet of interface dipoles was constructed, 80 nm in diameter and protruding 3 nm to each side of the interface. The center of this sheet contained a distribution of dipoles, while outside the center an averaged value was imposed. This sheet of interface dipoles was sufficiently large to compute the vacuum-level shift as sensed by charges that move up to 8 nm outward, starting at the center of this sheet/interface. ''Sufficiently large'' in this case means that the charge–QID interaction reached an approximately constant value away from the interface, as in Figure 4.

Acknowledgements

S.V. thanks Antoine Kahn for useful discussions. This work was partially supported by the European-funded projects MINOTOR (FP7-NMP-228424), MODECOM (NMP3-CT-2006-016434), and ONE-P (NMP3-LA-2008-212311). J.C. and D.B. are FNRS (Belgian National Fund for Scientific Research) Research Fellows.

Received: July 8, 2009
Revised: August 21, 2009
Published online: October 26, 2009

[1] A. Troisi, *Adv. Mater.* **2007**, *19*, 2000.
[2] E. A. Silinsh, V. Čápek, *Organic Molecular Crystals*, AIP Press, New York **1994**.
[3] V. Arkhipov, E. Emilianova, H. Bässler, *Phys. Rev. Lett.* **1999**, *82*, 1321.
[4] P. Peumans, S. R. Forrest, *Chem. Phys. Lett-* **2004**, *398*, 27.
[5] L. M. Andersson, O. Inganas, *Chem. Phys.* **2009**, *357*, 120.
[6] V. Arkhipov, H. Bässler, in *Thin Film Solar Cells* (Eds.: J. Poortmans, V. Arkhipov) Wiley, Chichester **2006**, chapter 8.
[7] V. D. Mihailetchi, L. J. A. Koster, J. C. Hummelen, P. W. M. Blom, *Phys. Rev. Lett.* **2004**, *93*, 216601.
[8] A. C. Morteani, P. Sreearunothai, L. M. Herz, R. H. Friend, C. Silva, *Phys. Rev. Lett.* **2004**, *92*, 247402.
[9] B. P. Rand, D. P. Burk, S. R. Forrest, *Phys. Rev. B* **2007**, *75*, 115327.
[10] D. Cheyns, J. Poortmans, P. Heremans, C. Deibel, S. Verlaak, B. P. Rand, J. Genoe, *Phys. Rev. B* **2008**, *77*, 165332.
[11] J. A. Barker, C. M. Ramsdale, N. C. Greenham, *Phys. Rev. B* **2003**, *67*, 075205.
[12] P. J. Bounds, R. W. Munn, *Chem. Phys.* **1981**, *59*, 47.
[13] S. Verlaak, P. Heremans, *Phys. Rev. B* **2007**, *75*, 115127.
[14] E. V. Tsiper, Z. G. Soos, *Phys. Rev. B* **2001**, *64*, 195124.
[15] J. E. Norton, J.-L. Brédas, *J. Am. Chem. Soc.* **2008**, *130*, 12377.
[16] D. Cheyns, H. Gommans, M. Odijk, J. Poortmans, P. Heremans, *Sol. Energy Mater. Sol. Cells* **2007**, *91*, 399.
[17] S. Yoo, B. Domercq, B. Kippelen, *Appl. Phys. Lett.* **2004**, *85*, 5427.
[18] I. Salzmann, S. Duhm, R. Opitz, R. L. Johnson, J. P. Rabe, N. Koch, *J. Appl. Phys.* **2008**, *104*, 114518.
[19] V. de Coulon, J. L. Martins, F. Reuse, *Phys. Rev. B* **1992**, *45*, 13671.
[20] R. Mitsumoto, T. Araki, E. Ito, Y. Ouchi, K. Seki, K. Kikuchi, Y. Achiba, H. Kurosaki, T. Sonoda, H. Kobayashi, O. V. Boltalina, V. K. Pavlovich, L. N. Sidorov, Y. Hattori, N. Liu, S. Yajima, S. Kawasaki, F. Okino, H. Touhara, *J. Phys. Chem. A* **1998**, *102*, 552.
[21] R. Feynman, *The Feynman Lectures on Physics*, Vol. *2*, Addison Wesley Longman, San Francisco **1970**.
[22] S. Verlaak, S. Steudel, P. Heremans, D. Janssen, M. S. Deleuze, *Phys. Rev. B* **2003**, *68*, 195409.
[23] H. Ishii, K. Sugiyama, E. Ito, K. Seki, *Adv. Mater.* **1999**, *11*, 605.
[24] I. Avilov, V. Geskin, J. Cornil, *Adv. Funct. Mater.* **2009**, *19*, 624.
[25] Y. Ge, J. E. Whitten, *Chem. Phys. Lett.* **2007**, *448*, 65.
[26] H. Vazquez, W. Gao, F. Flores, A. Kahn, *Phys. Rev. B* **2005**, *71*, 041308.
[27] S. Duhm, G. Heimel, I. Salzmann, H. Glowatzki, R. L. Johnson, A. Vollmer, J. P. Rabe, N. Koch, *Nat. Mater.* **2008**, *7*, 326.
[28] H. Ishii, A. Seko, A. Kawakami, K. Umishita, Y. Ouchi, K. Seki, *Mater. Res. Soc. Symp. Proc.* **2003**, *771*, 29.
[29] S. Kang, Y. Yia, C. Kima, S. Choa, M. Nohb, K. Jeong, C. Whanga, *Synth. Metals* **2006**, *165*, 32.
[30] S. Verlaak, C. Rolin, P. Heremans, *J. Phys. Chem. B* **2007**, *111*, 139.
[31] R. L. Martin, J. P. Ritchie, *Phys. Rev. B* **1993**, *48*, 4845.